RSC Advances

PAPER

Cite this: *RSC Adv.*, 2023, **13**, 21300

Controlled electrochemical surface exfoliation of graphite pencil electrodes for high-performance supercapacitors†

Ayman A. AbdelHamid, Abdelaziz Elgamouz and Abdel-Nasser Kawde *

A controlled surface exfoliation method for graphite pencil electrodes using an environmentally friendly, low cost and scalable electrochemical process is reported. A simple direct current power supply in a neutral medium is used for inducing graphene formation on the electrode surface in a controlled manner. The electrochemical properties of the surface exfoliated electrode are characterized, displaying a >300× increase in the electrochemical surface area and >50× decrease in the electrode resistance after exfoliation. The surface graphene layer is characterized using electron microscopy, Raman, infrared, X-ray photoelectron, and energy dispersive X-ray spectroscopies and X-ray diffractometry showing a fully exfoliated surface, formation of surface defects and mild surface graphene oxidation while maintaining an intact graphitic crystal structure. The surface exfoliated electrode is tested as a supercapacitor demonstrating more than 2 orders of magnitude improvement over non-exfoliated electrode in both 3-electrode and 2-electrode setups and achieving a high areal capacitance of ~54 mF cm^{-2}. The benign nature, low cost, scalability of our controlled surface exfoliation methodology, and its significant impact on the electrochemical properties of the electrode make it very promising for further investigation in various applications such as energy storage and conversion, sensors, and catalysis.

Received 13th June 2023
Accepted 5th July 2023

DOI: 10.1039/d3ra03952h

rsc.li/rsc-advances

Introduction

Energy storage has been in the spotlight of global affairs due to the rapid drive for electrification of the transport market and boosting renewable energy output. Both directions aim to reduce urban pollution and decrease reliance on fossil fuels, which are detrimental to the environment, a major cause of global warming and are not sustainable in the long term.[1,2] A supercapacitor (SC) is an energy storage system characterized by high power capability, fast charging, and very long cycle life,[3] acting as a bridge between conventional capacitors and batteries.[2,4,5] It is a vital component of the energy storage landscape, offering unique advantages and supplementing other energy storage systems. SCs have been used in various applications, especially those that require high-rate capability and long cycle life, such as acceleration and regenerative breaking in electric vehicles, backup power supply, electronic devices, healthcare, power tools, energy management, and solar energy harvesting.[1,6–8] Interestingly, they have been used lately in electric buses, demonstrating the huge potential market of this technology.[1,8] The main type of SCs is electric double-layer SCs (EDLCs), which store charge electrostatically on the electrode surface *via* Helmholz double-layer formation with no faradaic reactions involved. EDLCs require high electric conductivity and large surface area, two parameters that are well fulfilled by carbon.[4,9] Carbon is a very versatile material with a wide variety of allotropes, forms, surface areas, and textures. Moreover, it is of low cost, has high mechanical stability, and is environmentally friendly.[2,10] Graphite pencil electrode (GPE) is an inexpensive carbon-based electrode that is readily available and easy to process, modify and use in different applications. Its conductive graphitic nature allows for high electric conductivity, and its easy surface modification allows for the preparation of highly performing SC electrodes. Several studies have reported very promising SC performance using GPEs, applying different materials to enhance capacitance, such as polymers and/or inorganic nanoparticles.[4,11,12]

Graphene is one of the most promising SC carbon materials. The two-dimensional morphology of graphene, together with the sp^2 nature of its carbon structure, impart superior electrical, mechanical, chemical, and surface properties. The sp^2-bonded carbon allows for a very high electrical conductivity of 200 000 $cm^2\ V^{-1}\ s^{-1}$ and a highly mechanically strong structure with Young's modulus of 1 TPa. The layered morphology allows for high flexibility and a very large specific surface area of ~2630 $m^2\ g^{-1}$.[8,13–15] The exceptional electrical, mechanical, and surface properties of graphene make it an excellent candidate for EDLCs, whose sole requirements are high surface and electrical

Pure and Applied Chemistry Group, Department of Chemistry, College of Sciences, University of Sharjah, P.O. Box 27272, Sharjah, United Arab Emirates. E-mail: akawde@sharjah.ac.ae

† Electronic supplementary information (ESI) available. See DOI: https://doi.org/10.1039/d3ra03952h

conductivity. A single graphene sheet is estimated to store ~21 μF cm^{-2}, the highest attainable limit for any carbon material, with an equivalent theoretical specific capacitance of ~550 F g^{-1}.[15] The introduction of graphene to the surface of GPE could enhance its energy storage performance significantly. The modified electrode would retain the advantages of GPE as availability, low cost, and easy processing while using the superior properties of graphene on the surface. Although graphene deposition on the surface of GPE has been reported earlier,[16,17] such an approach requires separate synthesis of graphene oxide or graphene, followed by their deposition on the surface of GPE. This complicates the electrode preparation process and increases its cost and processing time. A more practical and efficient method would be partially exfoliating the GPE, forming surface graphene sheets. This would facilitate the electrode preparation and reduce its cost, critical parameters in the energy storage field. Direct surface exfoliation would also produce a more robust and stable electrode as the graphene is generated from the body of the GPE itself. Thus, it would be structurally better connected to the graphite core. A few reports have investigated this strategy for energy storage applications, mainly by Şahin's group, who could electrochemically graphenize the surface of GPE using cyclic voltammetry in concentrated acids, whereby the surface of GPE was exfoliated *via* acid-mediated oxidization during the anodic sweep forming graphene oxide that was then reduced to graphene during the cathodic sweep.[14] Moreover, they could introduce dopants to the exfoliated graphene by tuning the acid composition, such as introducing N,[10,18] S,[18] and P[19] dopants, using nitric, sulfuric, and phosphoric acids, respectively. Although this strategy achieved one-step GPE surface exfoliation with impressive SC performance, it has some limitations. The reliance on highly concentrated acids for the oxidative exfoliation of graphite is a critical challenge for large-scale applications due to the hazardous and corrosive nature of such acids, which would stifle and complicate industrial-scale applications. The second critical limitation is using cyclic voltammetry as the exfoliation technique which is only suitable for small-scale preparation in a 3-electrode cell and cannot be implemented on a large scale.

An ideal electrochemical GPE surface exfoliation process should use a low-cost, environmentally friendly electrolyte and a simple electrochemical technique that can be implemented industrially. $(NH_4)_2SO_4$ is a green and mild electrolyte that is very effective for the electrochemical exfoliation of graphite using a simple direct current (DC) power supply and has been used for the electrochemical synthesis of graphene.[20,21] The OH^- generated by water oxidation at the cathode at a high voltage bias conducted a nucleophilic attack on the graphite anode oxidizing the edges and grain boundaries of the graphite layers, allowing SO_4^{2-} and water intercalation, followed by SO_2 an O_2 gas generation that exfoliated the graphene sheets.[20] In this work, we modified this facile electrochemical setup for controlled GPE surface exfoliation instead of complete electrode exfoliation and applied the electrochemically surface-exfoliated GPE (SEGPE) as a high-performance SC electrode. The controlled GPE surface exfoliation could be achieved by tuning the bias voltage and exfoliation time. The GPE surface exfoliation process was optimized, achieving a >300× increase in the electrode's electrochemical surface area, together with a >50× decrease in the electrode's resistance. The exfoliated surface was studied using electron microscopy; Raman, infrared, X-ray photoelectron, and energy dispersive X-ray spectroscopies; and X-ray diffractometry, showing complete surface coverage by graphene sheets, surface defect generation, minor surface oxygenation, and stability of the graphitic crystalline structure, which are highly conducive properties for electrochemical applications. The optimal SEGPE was used as an SC electrode showing >2 orders of magnitude higher energy storage capacity, as compared to pristine GPE, both in half and full symmetric cells, demonstrating the high impact of our surface exfoliation technique for GPE applications.

The GPE surface exfoliation methodology reported herein bypassed the concentrated acids and complex techniques used in previous work, providing a path for large-scale implementation. We have also demonstrated the efficiency of our approach and its significant impact on the energy storage performance of GPE. These excellent results open the door for further applications of our surface exfoliation strategy for energy storage, sensing, and catalysis.

Experimental

Materials and chemicals

Pentel Hi-polymer HB Pencil leads (diameter = 0.5 mm) were used as the graphite pencil electrodes. $(NH_4)_2SO_4$, H_2SO_4, and $K_3[Fe(CN)_6]$ were purchased from Sigma-Aldrich. $K_4[Fe(CN)_6]\cdot 3H_2O$ and KCl were purchased from Wardle Chemicals and Eurolab, respectively. Ultrapure water was generated by Milli-Q Elix Essential® 5 system.

Surface exfoliation of GPE

A power supply (IRWiN POWERBASE V8) was used in the DC mode as the power source. The positive and negative terminals were connected to the GPE and Pt foil as anode and cathode, respectively. The two electrodes were immersed into a 0.1 M $(NH_4)_2SO_4$ solution at a distance of 2 cm and the GPE was maintained at a depth of 1 cm. Different voltages and exfoliation times were used to optimize the surface exfoliation process. The SEGPEs were washed well using ultrapure water after the exfoliation process, and the excess water was drained before further electrochemical testing. The SEGPEs were dried in an oven at 60 °C till completely dry before physicochemical characterization.

Physicochemical characterization

Scanning electron microscopy (SEM) was conducted using Tescan Vega3 fitted with an Oxford energy dispersive X-ray spectroscopy (EDX) analyzer. Fourier transform infrared (FTIR) and Raman spectroscopies were carried out using Bruker Tensor II and Renishaw inVia system, respectively. X-ray photoelectron spectroscopy (XPS) was carried out by Nexsa G2 Surface Analysis System (Thermo Scientific) with monochromatic Al Kα X-ray (1486.6 eV) and an ultra-high vacuum of

$\sim 10^{-9}$ mbar. Powder X-ray diffractometry (XRD) was performed using Bruker D8 Advance with a Cu source ($\lambda = 0.15406$ nm) at a voltage of 40 kV, current of 40 mA, using a step of 0.02° and time per step of 0.15 s.

Electrochemical testing

All electrochemical experiments were conducted using a CHI660E electrochemical workstation. Electrochemical characterization of SEGPEs was conducted in a three-electrode cell comprising GPE/SEGPE, Pt wire, and Ag/AgCl (1 M KCl) as working, counter, and reference electrodes, respectively, in an equimolar (5 mM) solution of $K_3[Fe(CN)_6]$ and $K_4[Fe(CN)_6]\cdot 3H_2O$ and 0.1 M KCl as the supporting electrolyte. Cyclic voltammetry (CV) was conducted at a voltage range of −0.4 V to 0.8 V using different scan rates. Supercapacitor testing was done in two and three-electrode setups in 1 M H_2SO_4 at a voltage range of 0–1 V using CV, and Galvanostatic charge–discharge (GCD) at different scan rates and current densities, respectively. Electrochemical impedance spectroscopy (EIS) was employed at a frequency range of 10^6 to 0.05 Hz and an amplitude of 5 mV. The three-electrode setup comprised GPE and SEGPE as working electrodes, Pt wire, and Ag/AgCl (1 M KCl) as counter and reference electrodes, respectively. The two-electrode setup had a symmetric configuration comprising two identical SEGPEs.

Results and discussion

The surface exfoliation process used in our work is based on an electrochemical system that has been developed for the electrochemical exfoliation of graphene from graphite sources. In such a system, a high voltage bias is applied by a DC power source in a 2-electrode setup, with the graphite source used as the anode. The OH^- generated by water electrolysis attacks the highly polarized graphite source, opening up the graphite structure for intercalation by the SO_4^{2-} anions together with H_2O molecules, undergoing reduction and oxidation and producing SO_2 and O_2 gases, respectively. In addition, CO gas is produced by carbon oxidation.[20,21] This gas generation is observed during the exfoliation process and is mainly responsible for tearing up the graphite structure resulting in graphene exfoliation. Our study modified this exfoliation process for surface-confined exfoliation of GPE rather than complete electrode exfoliation. In our modified methodology, graphite exfoliation is only confined to the surface of the electrode, leading to a surface-exfoliated electrode that is covered by graphene sheets (Fig. 1a). This approach is much more facile, less costly, and more environmentally and industrially friendly, as compared to previously reported methods for GPE surface graphenization that synthesized graphene oxide and graphene separately followed by their deposition on GPE[16,17] or used highly concentrated acids to conduct oxidative acid-mediated exfoliation.[10,14,19]

The exfoliation process was confined to the GPE surface by optimizing the exfoliation DC voltage and duration. To evaluate our surface exfoliation process, we used a $Fe(CN)_6^{3-/4-}$ redox couple which is a standard electrochemical highly reversible one-electron transfer system used to study the electrode surface.[2] CV was conducted in a solution of 5 mM $Fe(CN)_6^{3-/4-}$ in 0.1 M KCl at a voltage range of −0.4 V to 0.8 V and a scan rate of 100 mV for preliminary evaluation. Since our objective was only surface exfoliation, we started with a low voltage bias of 2.5 V; however, only minimal change of the CV profile of the $Fe(CN)_6^{3-/4-}$ redox couple was observed, as compared to the pristine GPE, even at a relatively long exfoliation duration of 300 s, where 2 broad redox peaks with high polarization were observed, indicating inefficient charge transfer process (Fig. S1a, ESI†). Thus, 2.5 V was deemed not high enough to induce sufficient surface exfoliation. Upon the application of a voltage bias of 5 V, the exfoliation process proceeded effectively, as was observed visually by the bubbling and graphene exfoliation at the GPE surface. After only 10 s, the $Fe(CN)_6^{3-/4-}$ CV profile changed significantly with the sharp redox peaks observed with much lower polarization ($\Delta E = 0.1$ V), as compared to ΔE of 0.65 V in the case of pristine GPE (Fig. 1b). More importantly, the current and area under the curve increased significantly, reflecting enhanced redox kinetics on the electrode surface, which could be attributed to the higher surface area, exposed surface graphene sheets, and also the surface functional groups generated during exfoliation, all of which provided significantly more electrochemically active sites for the redox reactions to take place. Such a phenomenon was augmented as the exfoliation time increased, where the peak current increased with the exfoliation duration with more than one order of magnitude increase over 300 s, as compared to pristine GPE. This was explained by the highly exfoliated electrode surface with graphene sheets covering the entire surface. The current response decreased at a long exfoliation time of 600 s indicating electrode consumption. At an exfoliation voltage of 10 V, the reaction proceeded much faster as noted by the sharper redox peaks and higher area under the curve, as compared to 5 V, till ∼90 s exfoliation time (Fig. 1c and S1b, ESI†). At longer exfoliation time than 90 s, the current response decreased significantly, as compared to 5 V. This could be explained by the very rapid exfoliation process at 10 V that supplied ∼5× power as compared to 5 V, thus the rate of change of electrode surface was much faster and the electrode was consumed very rapidly, thus complicating the controlled surface exfoliation process. Therefore, we concluded that 5 V would be the optimal voltage bias to use in our surface exfoliation strategy because it was high enough to induce very effective exfoliation but not too high to cause uncontrolled exfoliation.

The surface of pristine GPE appeared rather smooth under SEM (Fig. S2f, ESI†). After surface exfoliation for 1 s at 5 V, its roughness started to increase (Fig. S2g, ESI†), and at 10 s, exfoliated sheets could be observed (Fig. S2h, ESI†). The exfoliated graphene sheets covered the entire surface at 300 s (Fig. 1d, e and S2i, ESI†) and appeared much deeper into the core of the GPE at 600 s (Fig. S2j, ESI†). The morphology change agreed with the color and texture changes that could be observed visually, where the GPE color changed from light grey (Fig. S2a, ESI†) to dark grey and black at 1 s (Fig. S2b, ESI†) and

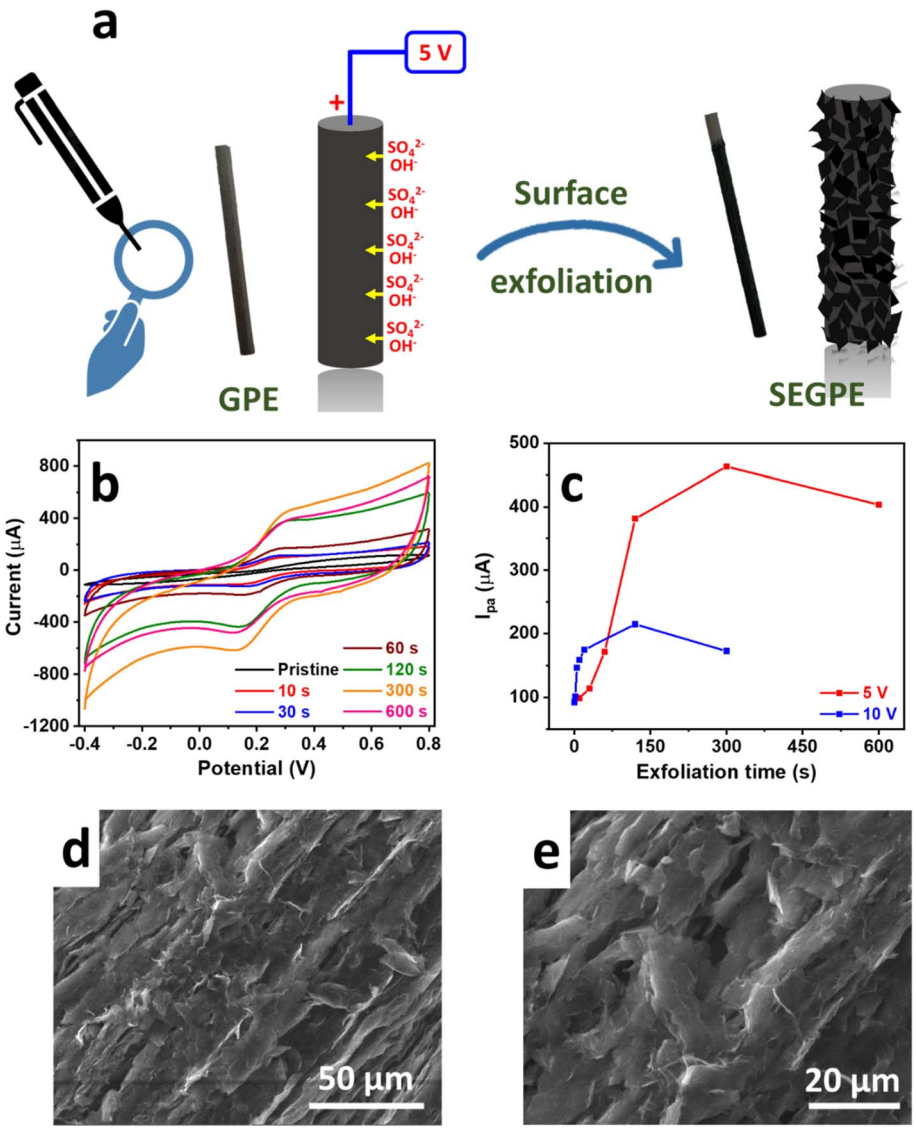

Fig. 1 (a) Scheme showing graphite electrochemical surface exfoliation process. (b) CV profiles of SEGPEs exfoliated at 5 V for different durations. (c) Comparison between CV anodic peak currents of SEGPEs exfoliated at 5 V and 10 V. CV in (b) and (c) was conducted in 5 mM $Fe(CN)_6^{3-/4-}$/0.1 M KCl at a scan rate of 100 mV s^{-1}. (d and e) SEM images of SEGPE exfoliated at 5 V for 300 s at different magnifications.

10 s (Fig. S2c, ESI†), respectively. At 300 s, the texture appeared rather rough, and surface etching was apparent (Fig. S2d, ESI†), and it became deeper at 600 s (Fig. S2e, ESI†). The color, texture, and morphological changes agreed with the results obtained electrochemically, where the surface exfoliation occurred gradually and seemed complete at 300 s, which matched the conclusion drawn earlier in the $Fe(CN)_6^{3-/4-}$ system.

GPE surface exfoliation was studied more extensively at a voltage bias of 5 V to further understand and optimize the process. SEGPEs exfoliated at 5 V were characterized *via* the $Fe(CN)_6^{3-/4-}$ to evaluate their electrochemical surface area and resistance change, as compared to the pristine GPE. CV was conducted at an increasing scan rate from 5 mV to 200 mV (Fig. S3, ESI†). As expected, the redox current increased linearly with the square root of the scan rate with a coefficient of determination (R^2) as high as 0.997 (Fig. 2a), indicating a diffusion-controlled redox reaction. The electrochemical surface area was calculated using the Randles–Sevcik equation (eqn (1)).[22,23]

$$I_{Pa} = 2.69 \times 10^5 \times n^{3/2} \times D^{1/2} \times v^{1/2} \times C \times A \quad (1)$$

where I_{pa} is the anodic peak current (A), n is the number of electrons transferred during the redox reaction, D is the diffusion coefficient (7.6×10^{-6} cm^2 s^{-1}), C is the concentration of the redox species (mol cm^{-3}), and A is the electroactive surface area in cm^2. SEGPEs exfoliated at 1 s, 10 s, 300 s, and 600 s have slopes of ~564, ~580, ~1034, ~2183, and ~2359, corresponding to electrochemical surface areas of 0.15 cm^2, 0.16 cm^2, 0.28 cm^2, 0.59 cm^2, and 0.64 cm^2, respectively. A significant increase in the electrochemical surface area was observed, especially at exfoliation durations of 300 s and 600 s, with an increase of

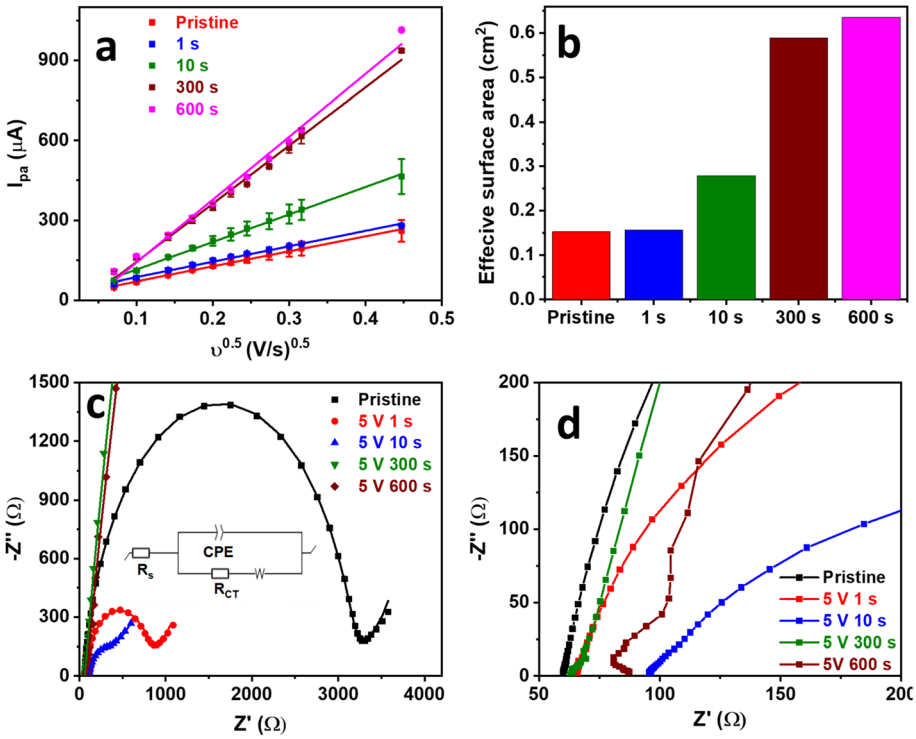

Fig. 2 (a) I_{pa} *vs.* $\nu^{0.5}$ plots, (b) effective surface area, (c) full-range (points: raw data, lines: fitting, inset: equivalent circuit used in fitting), and (d) partial-range Nyquist plots of pristine GPE and SEGPEs (5 V) tested in 5 mM $Fe(CN)_6^{3-/4-}$/0.1 M KCl.

~287% and ~319%, as compared to pristine GPE (Fig. 2b). The small increase in the electrochemical surface area beyond 300 s showed that the process was almost complete by that duration. Thus 300 s was concluded to be the optimal exfoliation time. In addition to the electrochemical surface area, surface roughness is an important measure of the electrode structure, where high surface roughness indicates three-dimensional (3D) structure formation, higher surface area, enhanced mass transfer, and thus improved charge storage capability. Surface roughness could be estimated using the fractal geometry approach reported earlier,[4] wherein diffusion-controlled systems, the fractal parameter (α) can be determined from the relationship between the peak current (I_p) and scan rate (ν) (eqn (2)).[4]

$$I_p \propto \nu^{\alpha} \quad (2)$$

As expected, the $\log I_p$ *vs.* $\log \nu$ plot of pristine GPE and SEGPE showed linear relationships with slopes of 0.45 and 0.59, respectively (Fig. S4, ESI†). The fractal dimension (D_f), which is a measure of surface roughness, could be calculated according to eqn (3).[4] D_f has a value of 2 for flat surfaces. A D_f value of less than 2 indicates inactive areas in the electrode surface, while values higher than 2 indicate high electrode surface roughness, 3D structure, and abundant microscopic domains. Pristine GPE had a D_f value of 1.9, indicating a flat surface with low surface activity. SEGPE displayed a higher D_f of 2.2 due to surface exfoliation that created a rough 3D surface.

$$D_f = 2\alpha + 1 \quad (3)$$

The SEGPEs were studied using EIS in the $Fe(CN)_6^{3-/4-}$ couple system to investigate the effect of surface exfoliation on their solution (R_s) and charge transfer (R_{CT}) resistances (Fig. 2c and d and Table 1).[4,12] R_s of the surface exfoliated electrodes did not show much change as compared to pristine GPE, reflecting no significant change in electrode conductivity. However, the surface exfoliation process had a major impact on R_{CT}, where R_{CT} decreased from ~3126 Ω for pristine GPE to 758.0 Ω and 312.1 Ω for SEGPE exfoliated for 1 s and 10 s, respectively. R_{CT} completely disappeared at 300 s and 600 s exfoliation, indicating the significant increase in the rate of charge transfer after surface exfoliation, mainly attributed to the large increase in the electrochemical surface area and the generation of electrochemically active sites due to exfoliation-induced surface functionalization. The >50-fold decrease in total resistance after surface exfoliation for 300 s showed the significant impact of

Table 1 EIS quantitative analysis (fitted using Randle's circuit) of SEGPEs exfoliated at 5 V for different durations

Exfoliation time (s)	R_s (Ω)	R_{CT} (Ω)	R_T (Ω)
0	59.9	3126	3186
1.00	64.7	758.0	822.7
10.0	98.6	312.1	410.7
300	63.0	0	63.00
600	83.3	0	83.30

our exfoliation methodology on the electrode's charge transfer kinetics.

To get an insight into the capacitive contribution of the huge increase of the redox current upon exfoliation. CV was conducted in 0.1 M KCl without the $Fe(CN)_6^{3-/4-}$ couple.[24] The capacitive component of the redox reaction increased significantly after surface exfoliation, accounting for ~72% of the total charge, compared to only ~2% in the case of pristine GPE (Fig. S5, ESI†). This could be attributed to the >300% increase in the electrochemical surface area upon surface exfoliation; in addition to the creation of surface functional groups, both phenomena could contribute to physical charge storage. This indicated the high potential of our surface exfoliation methodology for energy storage applications.

To understand the physical changes taking place during surface exfoliation, the composition, defects, and surface chemistry were characterized. EDX was used to study the composition of the SEGPE (Fig. 3a), especially the C/O ratio, which is a very good indicator of the oxygenated functional groups formed on the SEGPE surface. C/O ratio of pristine GPE was ~25% for pristine GPE and only decreased to ~23% for SEGPE exfoliated at 1 s; however, it underwent a major reduction to ~4% at 10 s and remained almost constant thereafter (Fig. S6a, ESI†). In other words, the oxygen content on the electrode's surface increased from 3.9 at% for pristine GPE to ~20 at% for SEGPE exfoliated at 10 s and 300 s, respectively. These results clearly showed the induction of surface oxygenated functional groups as a result of the exfoliation process and could have resulted mainly from the nucleophilic attack by the OH^- that induced the initial graphite oxidation and led to opening up its structure for later anionic intercalation and exfoliation. EDX spectrum and mapping images of SEGPE (5 V, 300 s) are shown in Fig. S6c and d, ESI,† displaying C and O as the major elements with atomic percentages of 79.2% and 19.6%, respectively. Minor amounts of Si and S were also detected, the former due to the inherent clay constituent in GPE, and the latter due to residual SO_4^{2-} groups from the exfoliation process. The Raman spectrum of graphite showed 3 main peaks at 1355.6 cm^{-1}, 1581.7 cm^{-1}, and 2724.6 cm^{-1} (Fig. 3b), corresponding to D, G, and 2D bands, originating from A_{1g} symmetry mode due to sp^3 carbon and defects, doubly degenerate phonon E_{2g} symmetry mode at the Brillouin zone center due to in-plane sp^2 vibration, and second order zone boundary phonons in the graphene structure, respectively.[25,26] SEGPE exhibited major changes in all 3 bands. The D band intensity increased significantly mainly due to the introduction of defects, sp^3 carbon, and oxygenated functional groups during exfoliation (Fig. 3b). The I_D/I_G ratio is a well-known defect indicator,[25,26] it has been shown to increase >3× from 0.36 till ~1.2 after 10 s exfoliation, in agreement with previous reports on graphene,[27,28] with minimal changes upon extending the exfoliation time (Fig. S6b, ESI†) with corresponding sp^2 carbon domains (L_a) of 12.1 nm for pristine GPE, and 3.7 nm, 4.1 nm, and 3.3 nm for SEGPE at 10 s, 300 s, and 600 s, respectively, as

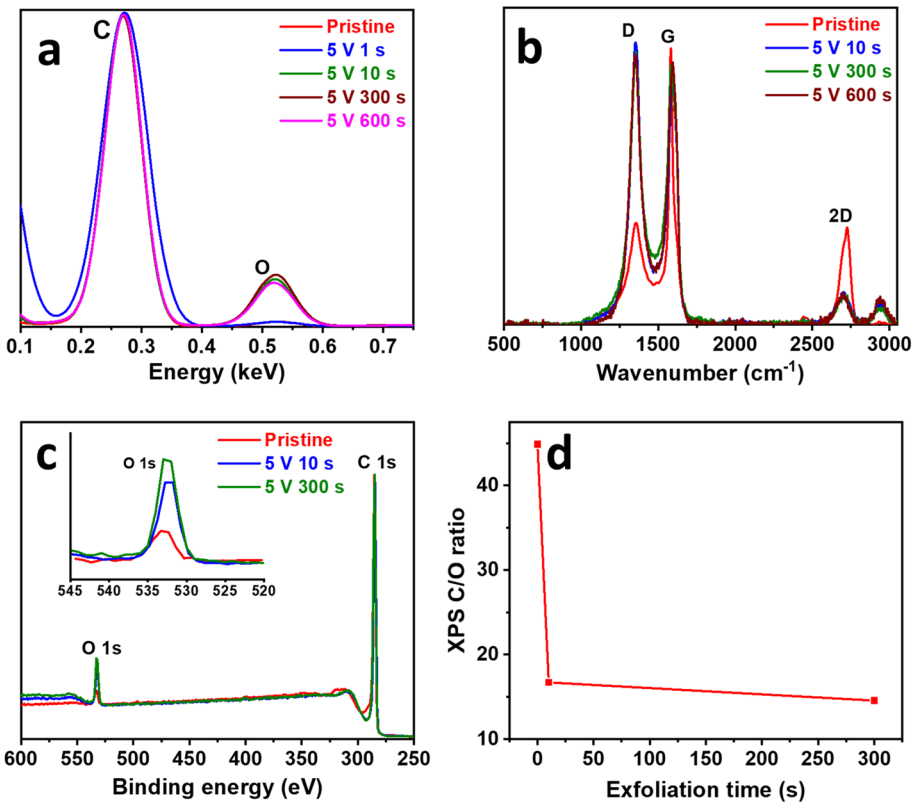

Fig. 3 (a) EDX, (b) Raman, and (c) XPS survey spectra of pristine GPE and SEGPEs (5 V). (d) XPS-derived C/O ratio *vs.* exfoliation time plot. Inset in (c): magnified O 1s region.

calculated using Kinghts empirical equation (eqn (4)),[29] which indicated major disruption of sp^2 carbon during exfoliation.

$$L_a = 4.35 \times (I_D/I_G)^{-1} \quad (4)$$

This observation agreed well with the C/O ratio displayed earlier and showed the correlation between the generated surface defects, disruption of large sp^2 carbon domains, and oxygenated functional group formation. Another change in the Raman spectra after exfoliation was that of the G band that showed peak broadening and blue shift, two phenomena that have been reported earlier and attributed to structural disorder, stress, and isolated double bonds[30,31] all of which could be associated with the reactions taking place during the exfoliation process. Finally, the 2D band intensity was reduced, which could be attributed to structural defects and disorders, and agreed with earlier reports.[26,31] This analysis demonstrated the effect of surface exfoliation on the structure of graphite indicating disorder, defects, sp^3 carbon, and oxygenated functional group formation. The decoration of SEGPE with oxygenated functional groups was analyzed using FTIR (Fig. S6e, ESI†). Pristine GPE only showed a peak at ~1616 cm^{-1} due to C=C bond.[19,32] At 10 s exfoliation, an extra small peak appeared at ~1235 cm^{-1}, which could be assigned to epoxy C–O bond,[32,33] and was more pronounced at 300 s exfoliation, which also showed 2 additional peaks at ~1446 cm^{-1} and ~954 cm^{-1} that could be assigned to CH_2 [34] and epoxy or peroxide[33] functional groups, respectively. The effect of the introduced functional groups on the structure of graphite has been examined by XRD (Fig. S6f, ESI†) by comparing the most intense (002) plane for pristine GPE and SEGPE at 10 s and 300 s. SEGPE (002) plane did not show any change in peak position or broadening, which indicated an intact graphitic crystalline structure with no change in interlayer spacing and no detectable disorder.[35–37] This could be explained by the confinement of the surface exfoliation to the GPE surface and thus no significant structural disorder was inflicted on the electrode and the core remained intact.

An in-depth compositional analysis of the electrodes' surface was done using XPS. Survey spectra showed 2 main peaks at ~285 eV and ~533 eV, corresponding to C 1s and O 1s, respectively (Fig. 3c).[38,39] The oxygen content increased as exfoliation proceeded with the C/O ratio decreasing from 44.9 for pristine GPE to 16.7 and 14.6 for SEGPE exfoliated at 10 s and 300 s (Fig. 3d), corresponding to an oxygen at% of 2.2, 5.7 and 6.4, respectively. C 1s core level spectra were analyzed to study the development of oxygenated functional groups over exfoliation time (Fig. S7a–c, ESI†). The spectra could be deconvoluted into 4 different components at 284.8 eV, 285.9 eV, 286.8 eV, and 288.8 eV, corresponding to C=C, C–O, C=O, and O–C=O groups, respectively.[39] It was observed that the ratio of the oxygenated carbon components, especially C–O, increased over exfoliation time from 0.32 for pristine GPE to 0.34 and 0.37 for SEGPE at 10 s and 300 s, respectively (Fig. S7d, ESI†). This analysis confirmed the formation of oxygenated groups on the exfoliated surface and agreed with the previous EDX, Raman, and FTIR results.

The gradual surface exfoliation process shown by SEM, which displayed the typical layered graphene structure with the fingerprint wavy and wrinkled morphology,[40] together with EDX and XPS analyses that showed carbon to be the major element, and Raman analysis that demonstrated a significant enhancement of the D band upon exfoliation and a 3× increase in I_D/I_G ratio to ~1.2, typical of graphene,[27,28] confirm electrode surface graphenization during our controlled surface exfoliation process. The ~84% and ~68% decrease in C/O ratio as calculated using EDX and XPS, respectively, upon surface exfoliation, in addition to the significant increase in oxygenated carbon species as detected by FTIR and XPS confirm the formation of oxygenated groups during the surface exfoliation process. The absence of change to the whole electrode's graphitic crystal structure could be explained by the controlled surface electrode treatment, which confined exfoliation and oxygenated group formation only to the surface layer while maintaining the graphitic highly conductive GPE core in the pristine condition to act as a directly attached electrode current collector.

The mechanism of our controlled surface exfoliation strategy is based on the electrochemical graphite exfoliation method for graphene synthesis;[20,21] however, the exfoliation voltage and time were controlled to confine the exfoliation process only to the surface. After applying the voltage bias between the graphite anode and Pt cathode, water was oxidized on the Pt surface, producing nucleophilic hydroxyl ions that attacked the positively-charged graphite, expanding its interlayer spaces. Such expansion allowed for the intercalation of electrolyte sulfate ions and water molecules into the graphite layers. The evolution of SO_2 and O_2 gases upon reduction and oxidation of SO_4^{2-} and H_2O resulted in graphite exfoliation. We have demonstrated that by fine-tuning the exfoliation voltage and time, the exfoliation process could be confined to the surface, thus changing the method outcome from graphene synthesis to controlled surface graphenization. We carefully optimized the exfoliation voltage and duration. We found that an exfoliation voltage of 5 V and duration of 300 s resulted in complete surface graphenization, together with the highest electrochemical activity, lowest resistance, and excellent capacitive properties.

The pristine GPE and SEGPE were tested for their supercapacitor performance initially using a 3-electrode setup in 1 M H_2SO_4. The open circuit potential (OCP) of the SEGPE was ~1.1 V, ~2.5× higher than that of pristine GPE (Fig. S8a, ESI†), mainly due to its higher surface area and functionalized surface. EIS is a very informative technique that sheds light on the conductivity and capacitive behavior of the electrodes. Nyquist plots showed the low resistance of both pristine and SEGPE (Fig. 4a), with negligible charge transfer resistance as shown by the non-existent semi-circles.[41] The intersection with the real impedance axis was taken as the total electrode resistance (R_T), including both solution and charge transfer resistances.[4,12] SEGPE had a slightly lower R_T of 18.12 Ω, as compared to 20.23 Ω shown by the pristine GPE. The Bode plots showed a higher phase angle of SEGPE at lower frequencies, as compared to pristine GPE (Fig. S8b, ESI†), indicating better

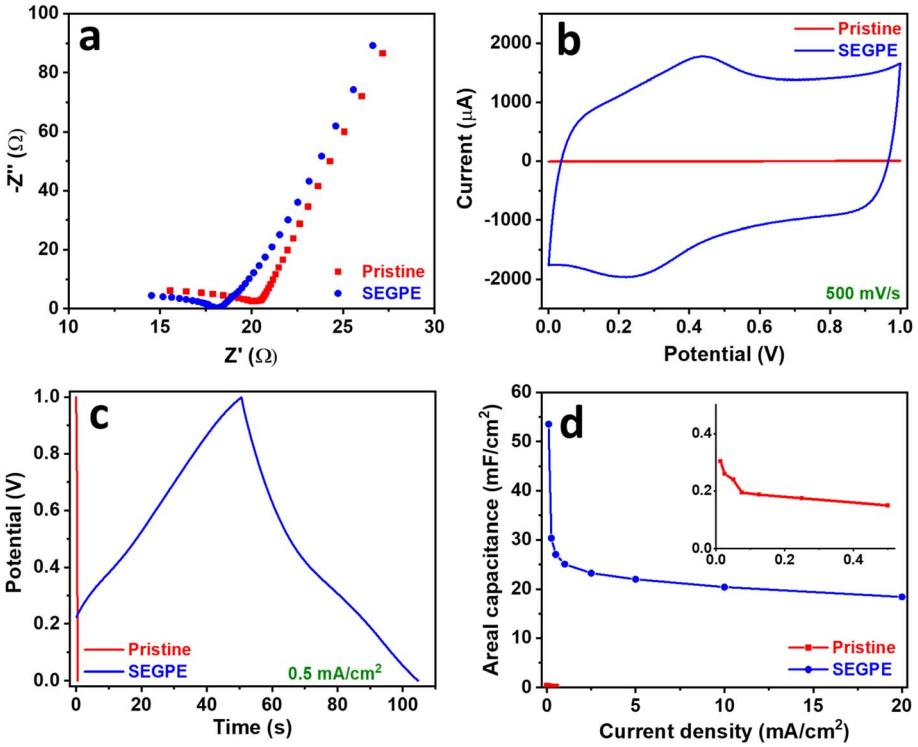

Fig. 4 (a) Nyquist, (b) CV, (c) GCD, and (d) areal capacitance *vs.* current density plots of pristine GPE and SEGPE (5 V, 300 s) in a 3 electrode cell. Inset in (d): magnified plot of pristine GPE.

capacitive behavior.[12,42] However, the phase angle decreased faster in SEGPE with increasing frequency, which also showed pseudocapacitive behavior.[42] This could be explained by the surface functional groups and defects introduced to the surface of the electrode during exfoliation that could have contributed to the pseudocapacitive charge storage,[43,44] and could also be attributed to the clay content in pencil leads,[45] which is mainly composed of silicates[46] that exhibit pseudocapacitive behavior,[47] and whose surface exposure could have been increased upon surface exfoliation.

CV was used to evaluate the electrode capacitance at a voltage range of 0–1 V. A typical rectangular-shaped CV was observed for pristine GPE (Fig. S9a, ESI†), which indicated an EDLC-type supercapacitor.[11] Only slight bumps could be seen at 0.2–0.4 V indicating a minor faradaic contribution, which could be attributed to the clay content present in the pencil leads, where the HB grade used in this study contains 26% clay.[45] The rectangular CV shape did not change at different rates till 500 mV s^{-1}, indicating good rate capability. However, a low current response of <10 μA was observed even at a high scan rate of 500 mV s^{-1}, indicating the limited energy storage capacity of pristine GPE. After surface exfoliation, the rectangular CV shape was maintained at all scan rates (Fig. S9b, ESI†), however, the faradaic contribution was more pronounced, which could be explained by the pseudocapacitive contribution of the oxygenated groups and the increased exposure of the pseudocapacitive clay content. The current response significantly increased as compared to pristine GPE, reaching ~2000 μA at 500 mV s^{-1} (Fig. 4b), showing more than 2 orders of magnitude improvement in capacitive energy storage over pristine GPE. This major charge storage increase is due to the complete coverage of the electrode surface by graphene sheets as demonstrated earlier, which enhanced the electrochemical surface area and thus increased the capacitive charge storage. Another reason could be the formation of surface oxygenated groups and the increased exposure of the GPE clay content during surface exfoliation, causing a significant pseudocapacitive contribution. The electrode charge storage capability was evaluated in more depth by GCD, and the areal capacitance was calculated using the discharge curve according to eqn (5).[10]

$$C = (i \times \Delta t)/(\Delta V \times A) \quad (5)$$

where C is the areal capacitance (mF cm^{-2}), i is the applied current applied (mA), Δt is the discharge time (s), ΔV is the working voltage (V), and A is the electrode surface area (cm^2). Volumetric capacitance (F cm^{-3}) was also calculated using eqn (5), using a volumetric current density in A cm^{-3} instead of an areal current density. The triangular-shaped GCD profiles of pristine GPE demonstrated the EDLC behavior (Fig. S9c and S10a, ESI†),[11] which agreed with the CV profiles shown earlier. Due to the limited storage capability of the pristine GPE, only low current densities could be used, ranging from 0.0125 mA cm^{-2} to 0.5 mA cm^{-2} (0.001–0.04 A cm^{-3}), showing discharge times of 24.1 s to 0.3 s, respectively (Fig. 4c and S9c, ESI†), corresponding to areal capacitances of 0.3 to 0.15 mF cm^{-2} (Fig. 4d), and volumetric capacitances of 0.025 to 0.012 F cm^{-3} (Fig. S11a, ESI†).

The ultimate energy storage parameters are energy density and power density. The first considers the electrode capacitance and working voltage, and the second the rate capability. Thus, the Ragone plot of energy density *vs.* power density is the most important display of the electrode energy storage performance. Energy and power densities were calculated according to eqn (6) and (7).[18,48]

$$E = (C \times \Delta V^2)/(2 \times 3.6) \quad (6)$$

$$P = (E \times 3.6)/\Delta t \quad (7)$$

where E is the energy density (μW h cm^{-2}) and P is the power density (mW cm^{-2}). Volumetric energy and power densities were also calculated using eqn (6), and (7), where C is the volumetric capacitance in F cm^{-3}, and E and P have the units of mW h cm^{-3} and W cm^{-3}, respectively. The areal energy densities of pristine GPE were calculated to be ∼0.04 μW h cm^{-2} and ∼0.02 μW h cm^{-2} at power densities of ∼0.006 mW cm^{-2} and 0.25 mW cm^{-2} (Fig. S9e, ESI†), corresponding to volumetric energy densities of ∼0.003 mW h cm^{-3} and ∼0.002 mW h cm^{-3} at power densities of ∼0.001 W cm^{-3} and ∼0.02 W cm^{-3}, respectively (Fig. S11b, ESI†). Another main factor for supercapacitor electrode evaluation is stability. We assessed the stability of pristine GPE by GCD over 5000 cycles at a current density of 0.125 mA cm^{-2}, showing impressive stability, retaining >99% of the capacity (Fig. S9f, ESI†). Although pristine GPE showed excellent EDLC behavior, its charge storage capability was very limited, as demonstrated by the low areal capacitance and corresponding energy density, making it impractical for real applications. On the other hand, after surface exfoliation, SEGPE showed much-enhanced performance, achieving ∼200× higher areal capacitance and energy density. The GCD profiles of SEGPE showed the typical EDLC triangular profiles (Fig. S9d and S10b, ESI†). However, minor plateaus were observed in the voltage range of 0.2–0.4 V, indicating major EDLC storage and a pseudocapacitive component in corroboration with the earlier CV analysis. Due to the better electrochemical properties of SEGPE, a higher range of current densities of 0.1–20 mA cm^{-2} (0.008–1.6 A cm^{-3}) could be applied. SEGPE showed discharge times of ∼536 s, ∼54 s, and 0.92 s (Fig. 4c and S9d, ESI†), corresponding to areal capacitances of 53.6, 27.1, and 18.4 mF cm^{-2} (Fig. 4d) at 0.1, 0.5 and 20 mA cm^{-2}, and volumetric capacitances of 4.4 F cm^{-3}, 2.2 F cm^{-3}, and 1.5 F cm^{-3} at 0.0082 A cm^{-3}, 0.041 A cm^{-3}, and 1.6 A cm^{-3}, respectively (Fig. S11a, ESI†). These results corresponded to areal energy densities of 7.4, 3.8, and 2.6 μW h cm^{-2} at power densities of 0.05, 0.25, and 10 mW cm^{-2} (Fig. S9e, ESI†) and volumetric energy densities of 0.61 mW h cm^{-3}, 0.31 mW h cm^{-3}, and 0.21 mW h cm^{-3} at power densities of 0.0041 W cm^{-3}, 0.020 W cm^{-3}, and 0.82 W cm^{-3}, respectively (Fig. S11b, ESI†). SEGPE displayed >180× improvement in areal capacitance and energy density over pristine GPE when compared at the same current density of 0.5 mA cm^{-2}, mainly due to the surface coverage by graphene sheets causing enhancement of electrode surface area. Similar to pristine GPE, SEGPE also showed excellent cycling stability over 5000 cycles (Fig. S9f, ESI†), with a slight improvement after ∼750 cycles, which could be explained by electrode surface activation due to better electrolyte diffusion and/or interaction that resulted in the exposure of more electroactive sites, a phenomenon that has been observed in previous studies.[49,50] These results showed the significant impact of our surface exfoliation strategy on the capacitive performance of the GPE. The large increase in surface area, exposure of inherent oxides, and surface functionalization during the exfoliation process were all factors in the >2 orders of magnitude enhancement in the energy storage capacity of the SEGPE. More importantly, our surface exfoliation strategy is

Table 2 Comparison of SEGPE supercapacitor performance with the literature[a]

Electrode	Electrolyte	Configuration	Areal capacitance (mF cm^{-2})	Current density (mA cm^{-2})	Ref.
Oxidized GPE (6H)	—	3 electrode	48.0	0.300	2
GPE (HB)	—	3 electrode	15.0	0.200	2
GPE (1H)	1 M Na_2SO_4	3 electrode	15.6	2.00	11
P-doped treated GPE (HB)	1 M H_2SO_4	3 electrode	49.7	0.500	19
S, N co-doped treated GPE	1 M H_2SO_4	3 electrode	71.5	10.0	18
Graphene coated Si	0.5 M Na_2SO_4	3 electrode	8.16	5.00 mV s^{-1} (scan rate)	51
Paper@CNT	3 M KOH	3 electrode	15.3	0.100	52
Paper@CNT@NCS	3 M KOH	3 electrode	38.3	0.100	52
Paper@CNT@NCS	3 M KOH	2 electrode	<2.00	0.400	52
Laser-induced graphene	1 M H_2SO_4	2 electrode	9.00	0.0200	53
Laser-induced graphene	LiCl/PVA	2 electrode	3.90	0.250	54
Graphite	H_3PO_4/PVA	2 electrode	10.4	0.100	55
This work	1 M H_2SO_4	3 electrode	53.6	0.100	This work
		3 electrode	30.4	0.250	
		3 electrode	23.3	2.50	
		2 electrode	4.70	0.125	
		2 electrode	4.31	0.469	
		2 electrode	3.75	3.13	

[a] CNT: carbon nanotubes. NCS: nickel cobalt sulfide. PVA: polyvinyl alcohol.

benign, facile, scalable, low-cost, and environmentally friendly, with no corrosive reagents and no need for high-cost electrochemical workstations, which have a tremendous impact when used as a platform for electrode preparation for energy storage and other electrochemical applications. We compared our work to the relevant literature (Table 2). Our SEGPE achieved 53.6 mF cm^{-2}, 30.4 mF cm^{-2}, and 23.3 mF cm^{-2} at 0.1 mA cm^{-2}, 0.25 mA cm^{-2}, and 2.5 mA cm^{-2}, respectively, in 3-electrode configuration, better than GPE (1H),[11] oxidized GPE (HB),[2] graphene-coated Si electrode,[51] and paper coated with carbon nanotubes (CNT) and metal sulfide/CNT composite.[52] In a 2-electrode setup, SEGPE achieved 4.70 mF cm^{-2}, 4.31 mF cm^{-2}, and 3.75 mF cm^{-2} at 0.13 mA cm^{-2}, 0.47 mA cm^{-2}, and 3.1 mA cm^{-2}, respectively, which was better or comparable to previously reported systems based on metal sulfide/CNT-coated paper,[52] laser-induced graphene,[53,54] and graphite.[55] Although we noted that some studies reported better performance by optimizing the pencil lead grades[2] and also doping the surface with P, S, and N,[18,19] our results are still comparable and can be further enhanced by adopting such strategies, which is currently under investigation. However, we would like to point out that we achieved such very promising results without using any corrosive acids using a simple DC power supply for surface exfoliation, unlike previous studies that relied on concentrated acids and high-cost electrochemical workstations, which make our approach more environmentally friendly, scalable and suitable for industrial application.

The 2-electrode setup is more representative of the supercapacitor performance and is closer to the practical device than the 3-electrode system, which tends to overestimate capacitance.[4] Therefore, we assembled a symmetric 2-electrode cell using identical SEGPEs.[4] Areal capacitance (C in mF cm^{-2}) in symmetric cells was calculated according to eqn (8) (volumetric capacitance in F cm^{-3} was also calculated using eqn (8), using a volumetric current density in A cm^{-3} instead of an areal current density in mA cm^{-2}),[48] while the energy and power densities were calculated according to eqn (6) and (7),[48] as explained earlier.

$$C = (2 \times i \times \Delta t)/(\Delta V \times A) \quad (8)$$

EIS of pristine GPE and SEGPE symmetric cells showed similar behavior as that in the 2-electrode setup. SEGPE symmetric cell has an R_T of 7.9 Ω, which was significantly lower than that of pristine GPE (36.9 Ω) (Fig. 5a), indicating better charge transfer capability of the surface exfoliated electrode.[56] Bode plots also showed a typical capacitive performance at low frequencies, with the SEGPE displaying a higher phase angle than pristine GPE, indicating better capacitive behavior (Fig. S8c, ESI†). CV and GCD of both pristine GPE and SEGPE (Fig. 5b, c and 6a, b) showed typical capacitor rectangular and triangular shapes, respectively. Pristine GPE symmetric cell could not be tested at CV scan rates higher than 50 mV s^{-1}, beyond which very high signal noise was observed, probably due to its limited charge transfer that could not tolerate high current currents. At 50 mV s^{-1}, only a small current of <0.3 μA was detected (Fig. S12a, ESI†). SEGPE symmetric cell could be tested up to 500 mV s^{-1} with the current response ~40 μA and

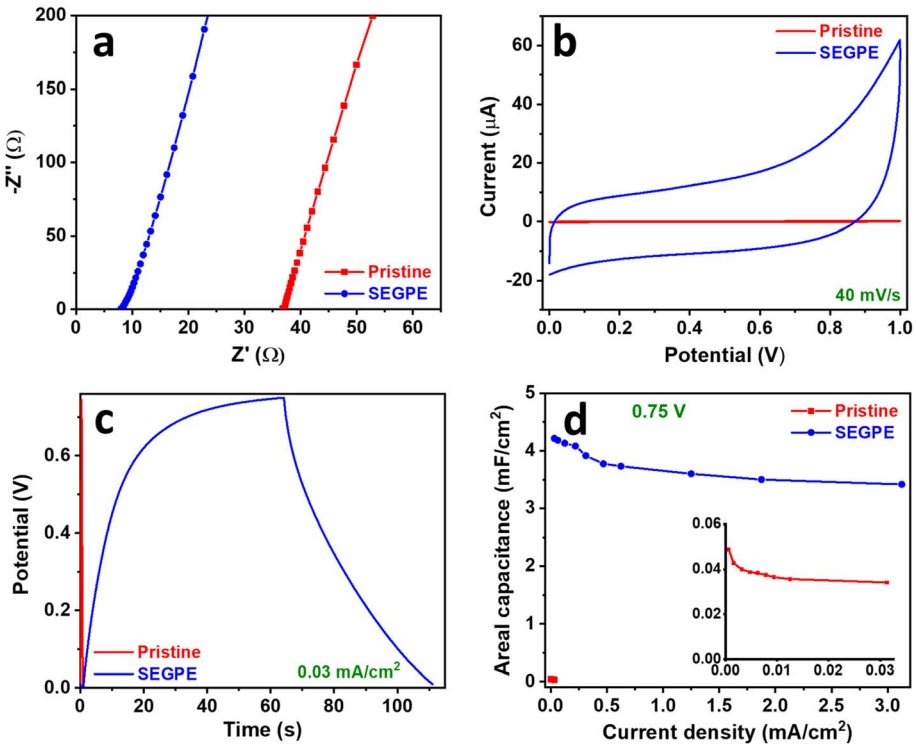

Fig. 5 (a) Nyquist, (b) CV, (c) GCD, and (d) areal capacitance *vs.* current density plots of pristine GPE and SEGPE (5 V, 300 s) in a symmetric cell. Inset in (d): magnified plot of pristine GPE.

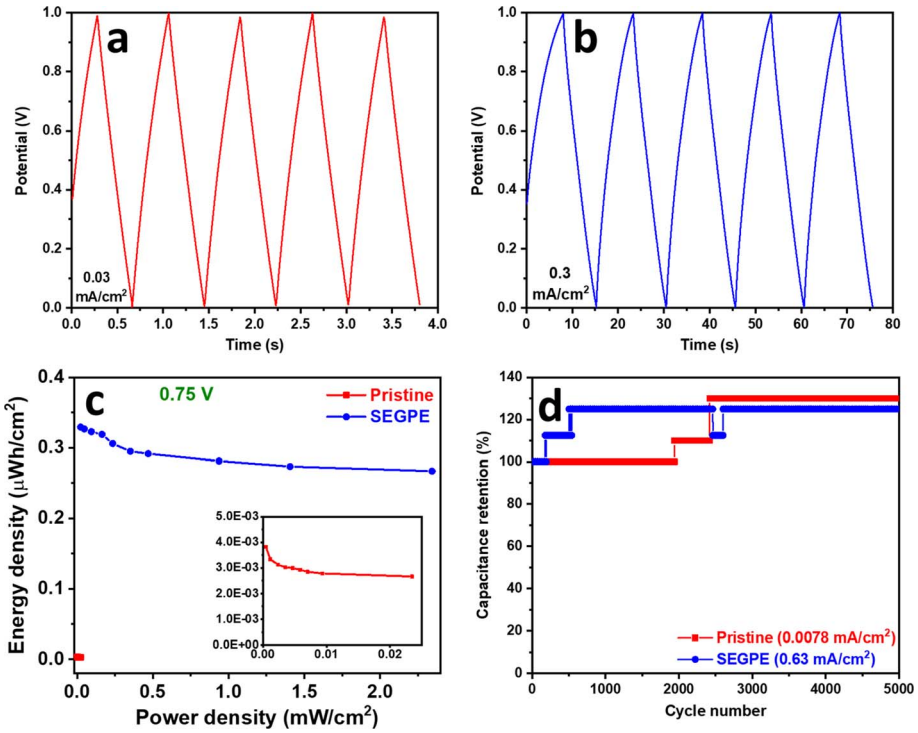

Fig. 6 (a and b) GCD profiles, (c) areal Ragone plot, and (d) stability profiles of (a) pristine GPE, (b) SEGPE (5 V, 300 s), and (c and d) pristine GPE and SEGPE (5 V, 300 s) in a symmetric cell setup. Inset in (c): magnified pristine GPE plot.

~250 μA at 40 mV s^{-1} and 500 mV s^{-1}, respectively, 200× better than pristine GPE (Fig. 5b and S12b, ESI†).

GCD of the symmetric cell was conducted in the voltage range of 0–1 V. Pristine GPE symmetric cell showed GCD discharge times of 43.1 s and 0.4 s (Fig. S12c, ESI†), corresponding to areal capacitances of 0.05 mF cm^{-2} and 0.02 mF cm^{-2} (Fig. S12e, ESI†), at current densities of 6 × 10^{-4} mA cm^{-2} and 0.03 mA cm^{-2}, and volumetric capacitances of 0.004 F cm^{-3} and 0.002 F cm^{-3} at current densities of 5 × 10^{-5} A cm^{-3} and 0.003 A cm^{-3}, respectively (Fig. S11c, ESI†). On the other hand, SEGPE

Table 3 Comparison between the electrochemical and energy storage parameters of pristine and SEGPE

Parameter	Pristine	SEGPE
3-electrode cell		
R_T (Ω)	20.2	18.1
Discharge time (s) at 0.500 mA cm^{-2}	0.300	54.1
Areal capacitance (mF cm^{-2}) at 0.500 mA cm^{-2}	0.150	27.1
Volumetric capacitance (F cm^{-3}) at 0.0408 A cm^{-3}	0.0122	2.21
Areal energy density (μW h cm^{-2}) at 0.250 mW cm^{-2}	0.0208	3.76
Volumetric energy density (mW h cm^{-3}) at 0.0204 W cm^{-3}	0.00170	0.307
OCP (V)	0.438	1.11
Symmetric cell (1 V)		
R_T (Ω)	36.9	7.88
Discharge time (s) at 0.0313 mA cm^{-2}	0.380	76.1
Areal capacitance (mF cm^{-2}) at 0.0313 mA cm^{-2}	0.0238	4.80
Volumetric capacitance (F cm^{-3}) at 0.00255 A cm^{-3}	0.00194	0.388
Energy density (μW h cm^{-2}) at 0.0313 mW cm^{-2}	0.00330	0.661
Volumetric energy density (mW h cm^{-3}) at 0.00255 W cm^{-3}	2.69 × 10^{-4}	0.0539
Symmetric cell (0.75 V)		
Discharge time (s) at 0.0313 mA cm^{-2}	0.41	50.6
Areal capacitance (mF cm^{-2}) at 0.0313 mA cm^{-2}	0.0342	4.22
Volumetric capacitance (F cm^{-3}) at 0.00255 A cm^{-3}	0.00279	0.344
Energy density (μW h cm^{-2}) at 0.0313 mW cm^{-2}	0.00267	0.329
Volumetric energy density (mW h cm^{-3}) at 0.00255 W cm^{-3}	2.18 × 10^{-4}	0.0269

symmetric cell showed GCD discharge times of 76.1 s and 0.6 s (Fig. S12d, ESI†), corresponding to areal capacitances of 4.8 mF cm^{-2} and 3.8 mF cm^{-2} (Fig. S12e, ESI†), at current densities of 0.03 and 3.13 mA cm^{-2}, and volumetric capacitances of 0.4 F cm^{-3} and 0.3 F cm^{-3} at current densities of 0.003 A cm^{-3} and 0.3 A cm^{-3}, respectively (Fig. S11c, ESI†). SEGPE symmetric cell showed >200× higher areal capacitance, as compared to pristine GPE symmetric cell at the same current density of 0.03 mA cm^{-2}, which was consistent with the CV results and also the results of 3-electrode setup. Interestingly, SEGPE symmetric cell also showed very good rate capability with ~80% capacitance retention over 2 orders of magnitude increase in current density from 0.03 mA cm^{-2} to 3.13 mA cm^{-2}. It achieved an energy density of 0.7 μW h cm^{-2} and 0.5 μW h cm^{-2} at power densities of 0.03 mW cm^{-2} and 3.13 mW cm^{-2} (Fig. S12f, ESI†), corresponding to volumetric energy densities of 0.05 mW h cm^{-3} and 0.04 mW h cm^{-3} at power densities of 0.003 W cm^{-3} and 0.3 W cm^{-3}, respectively (Fig. S11d, ESI†). Both pristine and SEGPE symmetric cells showed excellent stability over 5000 cycles (Fig. 6d), with both devices showing a capacitance increase over cycling, indicating induced activation, as explained earlier.

It was observed that SEGPE symmetric cell showed long charge curves at low current densities of 0.031–0.13 mA cm^{-2} (Fig. S12d†), while the GCD plots were balanced at higher current densities (Fig. 6b), indicating an overcharge process taking place at low current densities. Therefore, we conducted the GCD testing of symmetric cells at a lower voltage range of 0–0.75 V (Fig. S13a and b†). At a current density of 0.031 mA cm^{-2} (0.0026 A cm^{-3}), corresponding to a power density of 0.023 mW cm^{-2} (0.0019 W cm^{-3}), GPE and SEGPE showed discharge times of 0.41 s and 51 s (Fig. 5c), capacitances of 0.0342 mF cm^{-2} (0.0028 F cm^{-3}) and 4.22 mF cm^{-2} (0.344 F cm^{-3}) (Fig. 5d and S11e, ESI†), and energy densities of 0.0027 μW h cm^{-2} (2.18×10^{-4} mW h cm^{-3}) and 0.329 μW h cm^{-2} (0.027 mW h cm^{-3}), respectively (Fig. 6c and S11f, ESI†), with SEGPE showing >2 orders of magnitude higher performance, as compared to GPE. Moreover, SEGPE could maintain an excellent performance up to a current density of 3.13 mA cm^{-2} (0.255 A cm^{-3}), corresponding to a power density of 2.34 mW cm^{-2} (0.191 W cm^{-3}), achieving a capacitance of 3.42 mF cm^{-2} (0.279 F cm^{-3}) (Fig. 5d and S11e, ESI†) and an energy density of 0.267 μW h cm^{-2} (0.0218 mW h cm^{-3}) (Fig. 6c and S11f, ESI†). The differences between the supercapacitor performance of pristine GPE and SEGPE are highlighted in Table 3.

Conclusion

We have developed a new strategy for controlled surface exfoliation of GPE and demonstrated a significant impact of the surface exfoliated electrode in energy storage. The surface exfoliation parameters of voltage and time were optimized and the electrochemical properties of SEGPE were fully characterized, demonstrating a >300× increase in the electrochemical surface area and >50× decrease in the electrode's total resistance. This major improvement was mainly attributed to the complete electrode surface coverage by graphene sheets and the surface defects and functional groups induced by the surface exfoliation process. The optimal SEGPE was tested as a supercapacitor electrode in both 3-electrode and 2-electrode symmetric setups, demonstrating ~200-fold higher areal capacitance as compared to pristine GPE in both configurations. This significant improvement showed the high impact of our controlled surface exfoliation strategy for supercapacitor applications. The environmentally friendly, low cost and scalable process used in surface exfoliation in our work, together with the significant improvement in the electrochemical properties of the surface exfoliated electrode, also showed the high potential of our approach for various other applications, including energy storage and conversion, sensors, and catalysis.

Author contributions

Ayman AbdelHamid (A. A. A.): conceptualization, methodology, validation, formal analysis, investigation, data curation, writing – initial draft preparation, visualization; Abdelaziz Elgamouz (A. E.), Abdel-Nasser Kawde (A. K.): conceptualization, methodology, validation, formal analysis, investigation, resources, data curation, writing – original draft preparation, writing review & editing, visualization, supervision, project administration, funding acquisition.

Conflicts of interest

The authors declare no conflict of interest.

Acknowledgements

This research is funded by the Research Institute of Science and Engineering (RISE), University of Sharjah, Sharjah, United Arab Emirates, Seed Research Project No. (22021440119), V.C.R.G./R. 447/2022 and Collaborative Research Project No. (22021440122), V.C.R.G./R. 447/2022.

References

1 P. Manasa, S. Sambasivam and F. Ran, *J. Energy Storage*, 2022, **54**, 105290.
2 N. Vishnu, A. Gopalakrishnan and S. Badhulika, *Electrochim. Acta*, 2018, **269**, 274–281.
3 G. Xiong, P. He, Z. Lyu, T. Chen, B. Huang, L. Chen and T. S. Fisher, *Nat. Commun.*, 2018, **9**, 790.
4 S. Mondal, N. Aravindan and M. V. Sangaranarayanan, *Electrochim. Acta*, 2019, **324**, 134875.
5 A. A. AbdelHamid, X. Yang, J. Yang, X. Chen and J. Y. Ying, *Nano Energy*, 2016, **26**, 425–437.
6 W. Du, Z. Zhu, Y. Wang, J. Liu, W. Yang, X. Qian and H. Pang, *RSC Adv.*, 2014, **4**, 6998.
7 S. Banerjee, B. De, P. Sinha, J. Cherusseri and K. K. Kar, in *Handbook of Nanocomposite Supercapacitor Materials I: Characteristics*, ed., K. K. Kar, Springer Nature Switzerland AG, 2020.
8 M. Horn, B. Gupta, J. MacLeod, J. Liu and N. Motta, *Curr. Opin. Green Sustainable Chem.*, 2019, **17**, 42–48.

9 D. Sheberla, J. C. Bachman, J. S. Elias, C. J. Sun, Y. Shao-Horn and M. Dinca, *Nat. Mater.*, 2017, **16**, 220–224.
10 M. B. Arvas, M. Gencten and Y. Sahin, *Ionics*, 2021, **27**, 2241–2256.
11 R. Sha and S. Badhulika, *Nanotechnology*, 2019, **30**, 035402.
12 E. Karaca, D. Gökcen, N. Ö. Pekmez and K. Pekmez, *Int. J. Energy Res.*, 2019, **44**, 158–170.
13 S. W. Bokhari, A. H. Siddique, P. C. Sherrell, X. Yue, K. M. Karumbaiah, S. Wei, A. V. Ellis and W. Gao, *Energy Rep.*, 2020, **6**, 2768–2784.
14 H. Gürsu, M. Gençten and Y. Şahin, *Electrochim. Acta*, 2017, **243**, 239–249.
15 M. F. El-Kady, Y. Shao and R. B. Kaner, *Nat. Rev. Mater.*, 2016, **1**, 16033.
16 N. Baig, A. N. Kawde, A. Elgamouz, M. Morsy, A. M. Abdelfattah and R. Othaman, *RSC Adv.*, 2022, **12**, 2057–2067.
17 A. H. Oghli and A. Soleymanpour, *Biochem. Eng. J.*, 2021, **167**, 107920.
18 M. B. Arvas, H. Gürsu, M. Gencten and Y. Sahin, *ChemistrySelect*, 2022, **7**, e202200360.
19 M. B. Arvas, H. Gürsu, M. Gencten and Y. Sahin, *J. Energy Storage*, 2022, **55**, 105766.
20 K. Parvez, Z. S. Wu, R. Li, X. Liu, R. Graf, X. Feng and K. Mullen, *J. Am. Chem. Soc.*, 2014, **136**, 6083–6091.
21 K. Chen, D. Xue and S. Komarneni, *J. Colloid Interface Sci.*, 2017, **487**, 156–161.
22 M. Ibrahim, H. Ibrahim, N. B. Almandil, M. A. Sayed and A. N. Kawde, *Anal. Methods*, 2020, **12**, 2846–2857.
23 A. Ganguly and K. Y. Hwa, *Mater. Today Chem.*, 2022, **24**, 100862.
24 S. Ben-Amor, E. Vanhove, F. Sékli Belaïdi, S. Charlot, D. Colin, M. Rigoulet, A. Devin, N. Sojic, J. Launay, P. Temple-Boyer and S. Arbault, *Electrochim. Acta*, 2014, **126**, 171–178.
25 F. Yin, S. Wu, Y. Wang, L. Wu, P. Yuan and X. Wang, *J. Solid State Chem.*, 2016, **237**, 57–63.
26 B. Prakoso, Y. Ma, R. Stephanie, N. H. Hawari, V. Suendo, H. Judawisastra, Y. Zong, Z. Liu and A. Sumboja, *RSC Adv.*, 2020, **10**, 10322–10328.
27 B. Li, X. Jin, J. Lin and Z. Chen, *J. Cleaner Prod.*, 2018, **189**, 128–134.
28 A. S. AlShammari, M. M. Halim, F. K. Yam and N. H. M. Kaus, *Mater. Sci. Semicond. Process.*, 2020, **116**, 105140.
29 S. W. Park, B. Jang, H. Kim, J. Lee, J. Y. Park, S. O. Kang and Y. H. Choa, *Front. Chem.*, 2021, **9**, 699231.
30 A. Kaniyoor and S. Ramaprabhu, *AIP Adv.*, 2012, **2**, 032183.
31 D. Mhamane, W. Ramadan, M. Fawzy, A. Rana, M. Dubey, C. Rode, B. Lefez, B. Hannoyer and S. Ogale, *Green Chem.*, 2011, **13**, 1990.
32 M. B. Arvas, H. Gürsu, M. Gencten and Y. Sahin, *J. Energy Storage*, 2021, **35**, 102328.
33 D. He, Z. Peng, W. Gong, Y. Luo, P. Zhao and L. Kong, *RSC Adv.*, 2015, **5**, 11966–11972.
34 X. Colom, F. Carrillo, F. Nogués and P. Garriga, *Polym. Degrad. Stab.*, 2003, **80**, 543–549.
35 J. Lin, Y. Huang, S. Wang and G. Chen, *Ind. Eng. Chem. Res.*, 2017, **56**, 9341–9346.
36 B. Zhao, L. Jiang, X. Zeng, K. Zhang, M. M. F. Yuen, J.-B. Xu, X.-Z. Fu, R. Sun and C.-P. Wong, *J. Mater. Chem. A*, 2016, **4**, 14595–14604.
37 S. Hou, J. Li, X. Huang, X. Wang, L. Ma, W. Shen, F. Kang and Z.-H. Huang, *Appl. Sci.*, 2017, **7**, 852.
38 S. K. Bikkarolla, P. Cumpson, P. Joseph and P. Papakonstantinou, *Faraday Discuss.*, 2014, **173**, 415–428.
39 F. T. Johra, J.-W. Lee and W.-G. Jung, *J. Ind. Eng. Chem.*, 2014, **20**, 2883–2887.
40 B. Vasić, A. Zurutuza and R. Gajić, *Carbon*, 2016, **102**, 304–310.
41 A.-K. Hjelm and G. Lindbergh, *Electrochim. Acta*, 2002, **47**, 1747–1759.
42 J. S. Ko, M. B. Sassin, D. R. Rolison and J. W. Long, *Electrochim. Acta*, 2018, **275**, 225–235.
43 Y. J. Oh, J. J. Yoo, Y. I. Kim, J. K. Yoon, H. N. Yoon, J.-H. Kim and S. B. Park, *Electrochim. Acta*, 2014, **116**, 118–128.
44 S. Zhang, Y. Yang, R. Xiao, M. Yu, Y. Zhang, X. Sun, L. Lu, X. Wu and Y. Chen, *Appl. Clay Sci.*, 2021, **200**, 105821.
45 M. C. Sousa and J. W. Buchanan, *Comput. Graph. Forum*, 2000, **19**, 27–49.
46 M. He, Z. Wang, M. J. Moldowan and K. Peters, *Org. Geochem.*, 2022, **163**, 104331.
47 M. Wang, H. Wang, J. Wang and J. Zhang, *J. Electroanal. Chem.*, 2022, **905**, 115960.
48 H. Zhou, G. Han, Y. Xiao, Y. Chang and H.-J. Zhai, *J. Power Sources*, 2014, **263**, 259–267.
49 H. Gul, A. A. Shah and S. Bilal, *Polymers*, 2019, **11**, 1678.
50 S. Chandra Sekhar, G. Nagaraju, B. Ramulu, S. K. Hussain, D. Narsimulu and J. S. Yu, *Nano Res.*, 2019, **12**, 2597–2608.
51 T. H. Wu, C. T. Chang, C. C. Wang, S. Parwaiz, C. C. Lai, Y. Z. Chen, S. Y. Lu and Y. L. Chueh, *Nanoscale Res. Lett.*, 2018, **13**, 242.
52 K. Yu, W. M. Tang and J. Y. Dai, Flexible Solid-state Supercapacitors Using Paper-based Electrodes for Energy Storage, *presented at 2018 IEEE International Conference on Electron Devices and Solid State Circuits (EDSSC), 6–8 June 2018*, 2018.
53 Z. Peng, J. Lin, R. Ye, E. L. G. Samuel and J. M. Tour, *ACS Appl. Mater. Interfaces*, 2015, **7**, 3414–3419.
54 B. Xie, Y. Wang, W. Lai, W. Lin, Z. Lin, Z. Zhang, P. Zou, Y. Xu, S. Zhou, C. Yang, F. Kang and C.-P. Wong, *Nano Energy*, 2016, **26**, 276–285.
55 S. Zhu, Y. Li, H. Zhu, J. Ni and Y. Li, *Small*, 2019, **15**, 1804037.
56 P. Xu, Q. Gao, L. Ma, Z. Li, H. Zhang, H. Xiao, X. Liang, T. Zhang, X. Tian and C. Liu, *Carbon*, 2019, **149**, 452–461.